Journal of Atmospheric and Solar-Terrestrial Physics 105-106 (2013) 110–118

Contents lists available at ScienceDirect

Journal of Atmospheric and Solar-Terrestrial Physics

journal homepage: www.elsevier.com/locate/jastp

Automatic scaling of F layer from ionograms based on image processing and analysis

Haiyong Zheng [a,*], Guangrong Ji [a], Guoyu Wang [a], Zhenwei Zhao [b], Shaohong He [b]

[a] Ocean University of China, No. 238 Songling Road, Qingdao, Shandong 266100, China
[b] China Research Institute of Radiowave Propagation, No. 36 Xian Shandong Road, Qingdao, Shandong 266107, China

ARTICLE INFO

Article history:
Received 27 February 2013
Received in revised form
9 September 2013
Accepted 12 September 2013
Available online 21 September 2013

Keywords:
Ionogram automatic scaling
Ionospheric monitoring
Image processing
Image analysis

ABSTRACT

This paper presents a novel method for automatic scaling of the F layer from ionograms based on image processing and analysis techniques. The proposed method converts ionospheric vertical sounding data to a binary image. By extracting the F layer trace through segmentation of the F layer image, the ordinary and extraordinary traces used to scale ionospheric parameters can be separated automatically. We applied the method to ionograms recorded by the digital ionosonde developed at China Research Institute of Radiowave Propagation in which the ordinary and extraordinary modes are recorded together. Tests were performed on random ionograms with different qualities obtained at three ionospheric stations in different seasons and time and comparison of the results with those scaled by the standard manual method was given. The experiments show that the scaled parameters are valid and our method is feasible.

1. Introduction

Since the ionospheric F layer varies with disturbances and plays a major role in the reflection of radio waves, the condition of the F layer has been one of the key issues concerned with the design and operation of communication systems.

In the last three decades researchers have made many contributions developing computer programs to automatically scale vertical incidence ionograms, which principally include four steps: reducing the noise, forming the trace, identifying the trace, and scaling the parameters.

The ARTIST (Automatic Real-Time Ionogram Scaler with True-height) approach was to adaptively threshold the ionogram to remove background noise, reduce echoes to edgels corresponding to the leading edge of the echo, string echoes into traces, identify traces and determine their characteristics using information of wave polarization based on hyperbolic curve fitting (Reinisch and Huang, 1983; Reinisch et al., 2005; Galkin and Reinisch, 2008). The Autoscala method developed by Scotto (2001) adopted a correlation-based curve fitting algorithm to identify and scale F2 layer (Scotto and Pezzopane, 2002, 2008; Pezzopane and Scotto, 2010), Es layer (Scotto and Pezzopane, 2007) and F1 layer (Pezzopane and Scotto, 2008) traces of the ionograms without polarization information. Fox and Blundell (1989) designed a system relying on an ionosonde only able to record ordinary ray echoes, by which a trace is formed using successive mathematical extrapolations. The algorithm developed by Igi et al. (1993) did not distinguish between ordinary and extraordinary mode components and it was based on parabolic and hyperbolic curve fittings. Tsai and Berkey (2000) developed a method according to the concepts of fuzzy segmentation and connectedness. Ding et al. (2007a,b) presented a method based on empirical orthogonal function (EOF) analysis to automatically scale the F2 layer parameters. The algorithm developed by Liu et al. (2009) was based on an IRI model in combination with the methods of fuzzy theory, constraint extrapolations and ARTIST.

The current methods of ionogram automatic scaling are mainly based on the mechanism of ionospheric echo signals, and try to combine the empirical data and model through fitting and extrapolation to identify each layer trace for scaling automatically, and which may not be easily applied to different ionosondes at different longitudes and latitudes in different seasons and time directly. This paper presents a novel method for automatic scaling of the F layer from ionograms based on image processing and analysis techniques (Fig. 1). The method converts the sounding data recorded by an ionosonde to a gray-level image and reduces the impulse noise through image preprocessing and binarization. By segmentation of the F layer image with the removal of the F layer multiple reflections according to the characteristics of ionospheric structure, the F layer trace can be extracted by image skeletonization and mathematical morphology. Then the F layer parameters are scaled automatically based on the least square polynomial fitting and image projection. This method can implement

* Corresponding author. Tel.: +86 53266781215.
E-mail addresses: zhenghaiyong@gmail.com, zhenghaiyong@ouc.edu.cn (H. Zheng), grji@ouc.edu.cn (G. Ji), gywang@ouc.edu.cn (G. Wang), zhaozw22s@163.com (Z. Zhao), shaohonghe@hotmail.com (S. He).

1364-6826/$ - see front matter © 2013 Elsevier Ltd. All rights reserved.
http://dx.doi.org/10.1016/j.jastp.2013.09.007

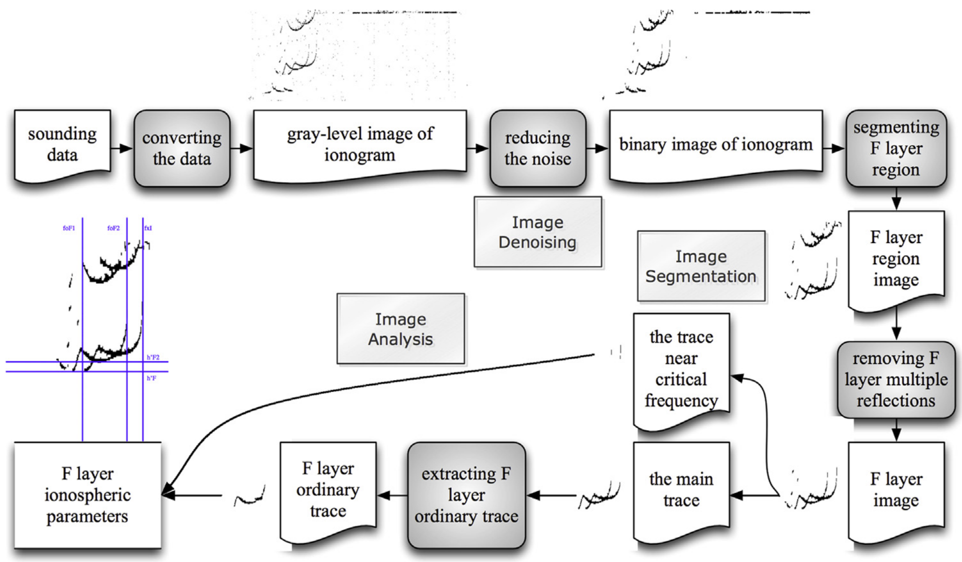

Fig. 1. The method proposed in this paper to scale F layer from ionograms automatically.

automatic scaling for ionograms recorded by different digital ionosondes without historical or empirical data and model and can separate the ordinary and extraordinary traces without polarization information. In this paper tests were performed on random ionograms with different qualities obtained at three different ionospheric stations in different seasons and time by the digital ionosondes developed at China Research Institute of Radiowave Propagation and comparison of the results with those obtained by the standard manual method was given.

2. Converting the sounding data to a binary image

2.1. Converting the sounding data to a gray-level image

The sounding data consists of a set of m vectors of n dimensions that can be converted to a matrix A of m rows and n columns according to the sounding mechanism. The matrix A can be transformed into a gray-level image with a size of $m \times n$, where the abscissa (horizontal direction x) represents frequency f (MHz), and the ordinate (vertical direction y) represents virtual height h' (km), whose number is defined by the following formulas:

$$f = n \times f_{step} + f_{start} \text{ (MHz)} \tag{1}$$

$$h' = m \times h_{step} \text{ (km)} \tag{2}$$

where f_{step} is the frequency step of the sounding and the frequency starts from f_{start}, while h_{step} is the height resolution at which the sounding has been recorded. The gray-level value of each pixel represents the echo amplitude received by the ionosonde, and the higher the value, the stronger the echo amplitude received by the ionosonde.

The gray-level image converted from the data received by the digital ionosonde we used in this paper is of size 320×640 with the intensity value of each pixel in the range [0, 255], and f_{start} is 1, h_{step} is 2.5 while f_{step} is adjustable such as 0.025 and 0.03.

2.2. Image preprocessing and binarization

In order to extract each layer trace of an ionogram for automatic scaling, image processing techniques were applied to remove noise from the gray-level ionograms which contain the echo signals as well as the impulse noise caused by the ionosonde or electromagnetic interference. Usually, the amplitude of echo signals is higher than that of the impulse noise. To eliminate the impulse noise, the smoothing spatial filtering on ionograms followed by a threshold was adopted in our method. Specifically, we used the morphological closing operation (Gonzalez and Woods, 2008, Chapter 9) to smooth sections of the trace contours while repairing the small discontinuities in traces and the max filter (Gonzalez and Woods, 2008, Chapter 3) to enhance the traces while suppressing the noise, and then applied the OTSU (Otsu, 1979) adaptive threshold method to eliminate the noise yielding the binary ionogram.

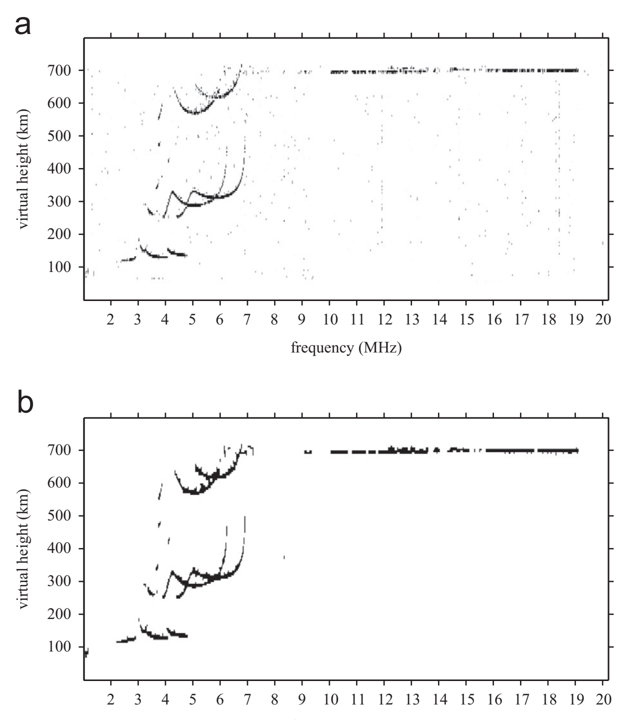

Fig. 2. (a) Gray-level image of ionogram recorded on 1st February 2010 at 11:30 am local time by the ionosonde installed at Xinxiang station. (b) The binary image of the ionogram (a).

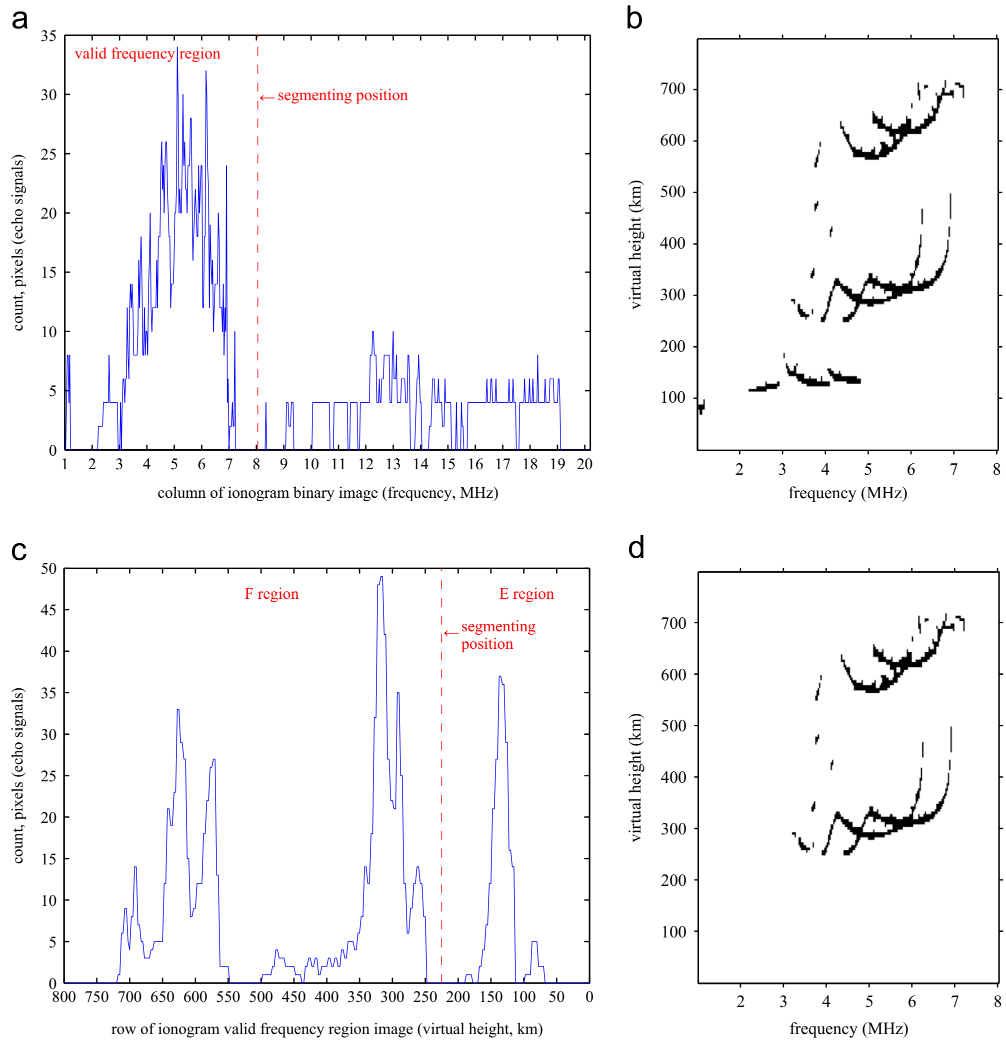

Fig. 3. Segmenting the F region image from Fig. 2b. (a) The vertical projection integral curve of the ionogram binary image Fig. 2b, where the horizontal axis represents the column of the ionogram binary image (frequency) and the vertical axis represents the sum of corresponding pixels (echo signals). (b) The segmented valid frequency region image containing the E region image and the F region image of the ionogram according to (a). (c) The horizontal projection integral curve of the ionogram valid frequency region image (b), where the horizontal axis represents the row of the ionogram valid frequency region image (virtual height) and the vertical axis represents the sum of corresponding pixels (echo signals). (d) The segmented F region image containing F layer image and F layer multiple reflections of ionogram according to (c).

Fig. 2 is an example of the experimental results. It can be shown that the proposed techniques of image preprocessing and binarization did improve the image quality of ionogram significantly without computational complexity, while the key information of the trace was kept and the noise was reduced.

3. Segmenting F layer image

3.1. Segmenting F region image

Generally the frequency band of valid ionospheric echo signals does not occupy the entire frequency range of ionogram, as shown in Fig. 2b, where the right part (high frequency region) is in fact strong interference caused by the ionosonde we used due to the limitation of this ionosonde, which cannot be removed by the OTSU method. So it is important to remove the high frequency region with strong interference by image segmentation to simplify the subsequent computations in trace extraction and identification. We used the image projection method to segment the F region image, specifically, the vertical projection of the binary ionogram means to sum the echo signals in each frequency channel forming the integral curve, while the horizontal projection of the binary ionogram means to sum the echo signals in each virtual height forming the integral curve.

Considering that the ionospheric echo signals are usually concentrated and continuous but spaced with the high-frequency strong interference echo signals, we combined the image projection method and ionospheric structural characteristics to segment the valid frequency region image from the ionogram binary image. Fig. 3b shows the segmented valid frequency region image removing the high-frequency strong interference from the ionogram binary image (Fig. 2b) according to its vertical projection (Fig. 3a).

Since there always exists an interval on the horizontal projection integral curve between the E region and the F region because of the ionospheric E–F valley, we can further segment the F region. In order to separate F region from E region especially Es layer effectively, the highest row with minimal integral value of horizontal projection between 150 km and 250 km, which means the first interval below the F layer trace, will be chosen as the segmenting position, and if there appears continuous zero integral values a suitable higher row of the range will be chosen. From Fig. 3c, it can be seen that the E–F valley of ionogram (Fig. 3b) with interval ranged from 190 km to 247.5 km and 225 km was chosen

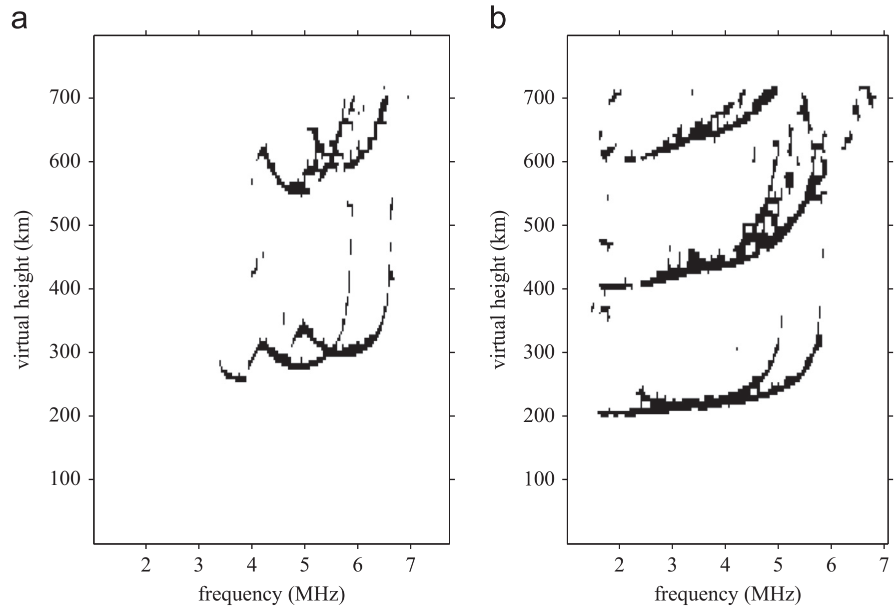

Fig. 4. (a) Ionogram of the trace near the F layer critical frequency close to the second-order reflection in the horizontal direction recorded on 1st February 2010 at 11:00 am local time by the ionosonde installed at Xinxiang station. (b) Ionogram of the trace near the F layer critical frequency overlapped with the second-order reflection in the horizontal direction recorded on 18th February 2010 at 6:30 pm local time by the ionosonde installed at Xinxiang station.

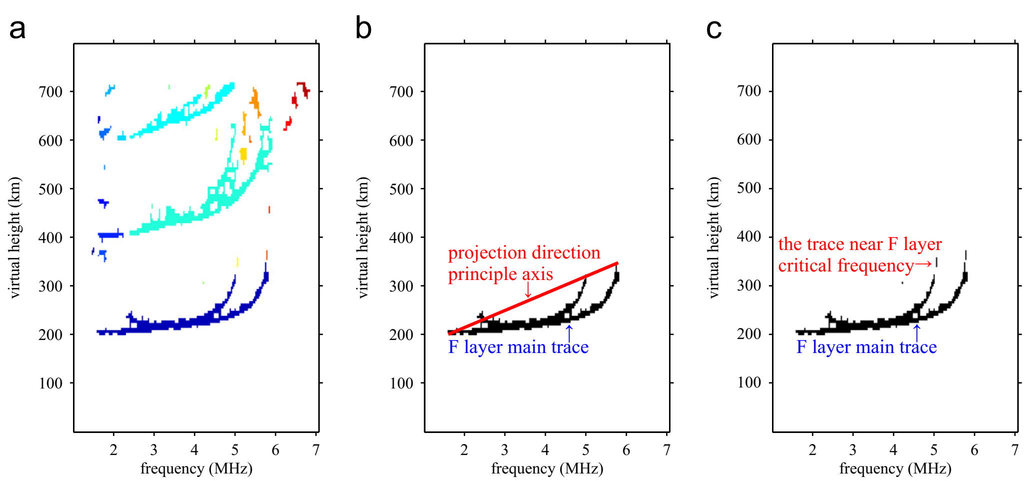

Fig. 5. Removing F layer multiple reflections from Fig. 4b. (a) 8-Connected components labeled F region image of ionogram Fig. 4b. (b) The principle axis (the inclined red line) of the F layer main trace indicating the projection direction for image projection to remove the F layer multiple reflections. (c) F layer image containing F layer main trace and the trace near F layer critical frequency. (For interpretation of the references to color in this figure caption, the reader is referred to the web version of this paper.)

as the segmenting position yielding the segmented F region image (Fig. 3d).

3.2. Removing F layer multiple reflections

The F layer multiple reflections are usually incomplete second-order reflections at the level of double altitudes (Figs. 3d and 4a), and sometimes third-order reflections (Fig. 4b). These multiple reflections are due to the "multiple bounces" of the signal between the ionosphere and the Earth and do not represent additional higher layers (Scotto and Pezzopane, 2008), which can mislead the extraction of the F layer trace as well as the automatic scaling. Because of the typical vertical asymptotical shape of the F2 trace, the traces near the F layer critical frequency are usually very close to the second-order reflections in the horizontal direction (Fig. 4a) or even overlapped in the horizontal direction (Fig. 4b), preventing the separation of the primary and multiple F layer traces.

However, the F layer trace and the trace of the F layer multiple reflections are usually similar in the shape as well as the growing trend on frequency, so that there must be such an inclined direction along the growing trend to separate them optimally. According to the morphological characteristics, the F layer trace can be divided into two parts: the larger connected trace containing most of the F layer information called the main F layer trace and the remaining trace called the trace near the F layer critical frequency (Fig. 5c). Therefore, the inclined direction to remove F layer multiple reflections in terms of the principle axis can be determined by the diagonal of the minimum bounding rectangle of the main trace.

The connected components labeling method (Samet and Tamminen, 1988) was adopted to find the principle axis of the main F layer trace based on the ionospheric structural characteristics. Specifically, we used connected components labeling (Fig. 5a) to find the maximum connected region in the range of the F layer and the diagonal of the minimum bounding rectangle of the maximum

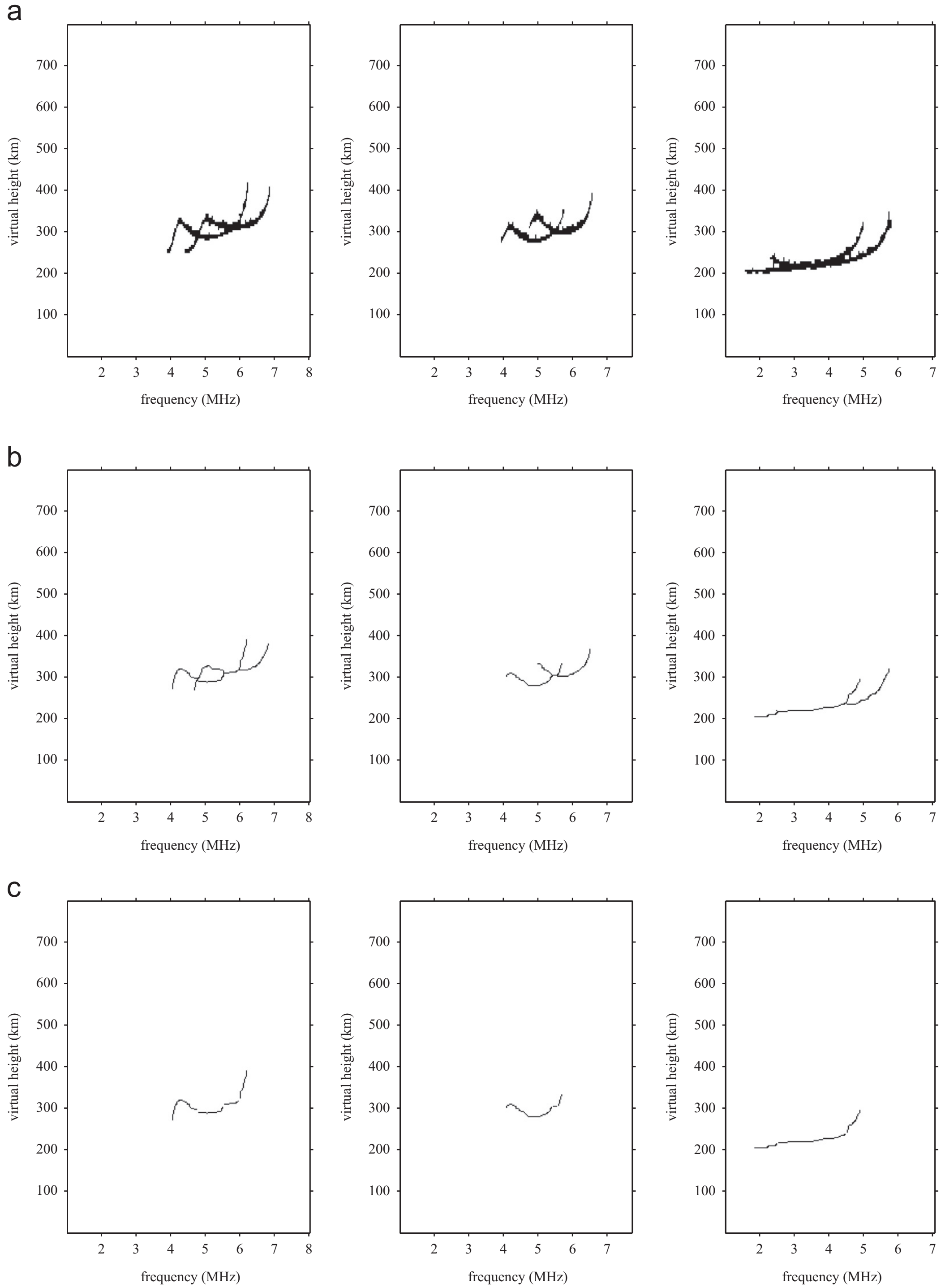

Fig. 6. Three standard F layer main trace configurations, where the ordinary trace always appears first and the ordinary and extraordinary traces interchange up and down after junction points. (a) The segmented F layer main traces of ionograms from Xinxiang station recorded on 1st February 2010 at 11:30 am local time, 1st February 2010 at 11:00 am local time, and 18th February 2010 at 6:30 pm local time, from left to right. (b) The corresponding skeletons of (a). (c) The corresponding extracted ordinary trace skeletons from (b).

connected region to determine the principle axis (Fig. 5b). Then the F region image can be projected along the principle axis direction to identify the F layer trace and the trace of the F layer second-order reflection according to the virtual height range and morphological similarity. The first minimal integral value below the second-order reflection along the projection direction was chosen to separate the F layer trace from the trace of the F layer multiple reflections. As shown in Fig. 5 the algorithm can eliminate the multiple reflections from ionograms without any change of the F layer trace.

4. Extracting F layer ordinary trace skeleton

The separation of ordinary and extraordinary traces in the main F layer trace is the key step for automatic scaling, especially for the ionograms recorded by ionosondes in which the ordinary and extraordinary modes are recorded together. Considering the features of the F layer ordinary trace shown in Fig. 6a, we combined image skeletonization (Zhang and Suen, 1984) with image analysis techniques to extract the main F layer trace and the ordinary trace

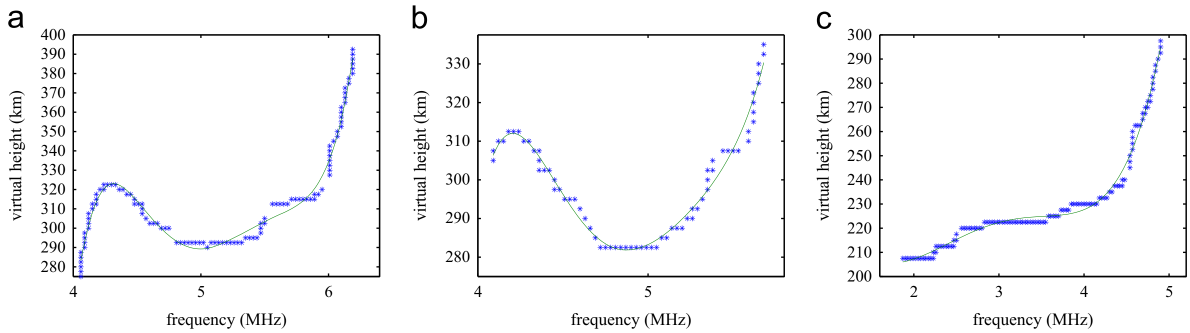

Fig. 7. The corresponding curve fitting results of the three standard F layer ordinary trace skeletons Fig. 6c.

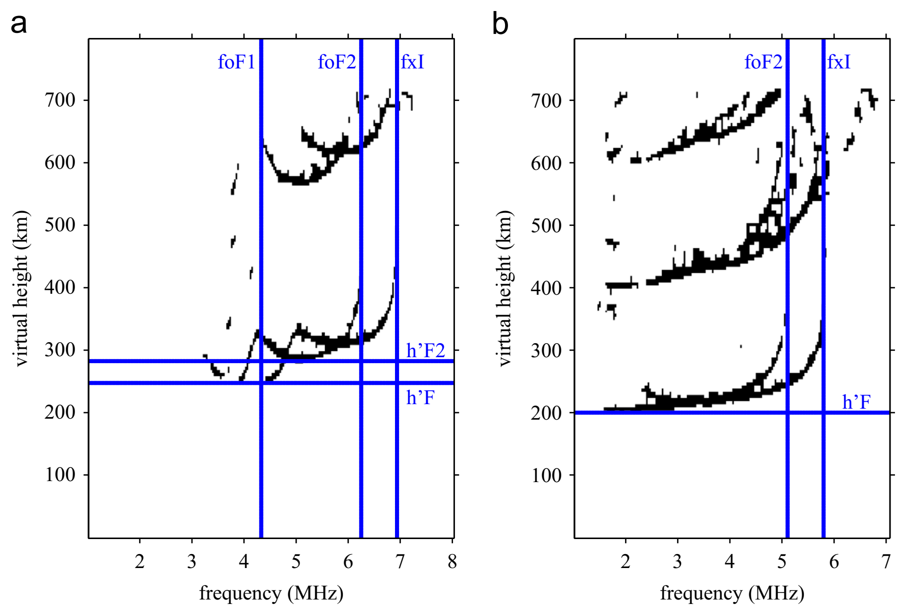

Fig. 8. F layer automatic scaling results with scaled parameters marked in blue horizontal and vertical lines. (a) A daytime ionogram from Xinxiang station at 11:30 am local time on 1st February 2010. (b) A nighttime ionogram from Xinxiang station at 6:30 pm local time on 18th February 2010. (For interpretation of the references to color in this figure caption, the reader is referred to the web version of this paper.)

skeleton shown in Fig. 6b and c respectively. Specifically, we detected the end points and junction points (Ji et al., 2010) of the main F layer trace skeleton, and then scanned the skeleton from left to right to identify and extract the ordinary trace skeleton according to the following characteristics: (1) ordinary trace appears first; (2) ordinary and extraordinary traces interchange up and down after junction points.

The information we used to separate the ordinary and extraordinary traces is the upper and lower structural relation of the traces divided by their junction points, which makes it still valid if the two components are dissimilar. But if unusual situation occurs, such as the ordinary and extraordinary traces are parallel without any junction point, the error of separation will be caused by this method. And we will consider using the morphological characteristics of the traces to recognize these unusual situations in the future.

5. F layer automatic scaling

foF1, h'F and h'F2 can be scaled from the extracted F layer ordinary trace skeleton by fitting the least squares polynomial model (Fig. 7).

foF2 and fxI can be scaled from the trace near the F layer critical frequency of the ordinary and extraordinary waves by the image projection method based on mathematical morphology (Gonzalez and Woods, 2008, Chapter 9) and line detection according to the typical vertical asymptotical shape of the F2 trace. We applied a larger elongated structuring element to dilate and a smaller elongated structuring element to erode sequentially on the trace near the F layer critical frequency completing the disconnected trace, and used the radon transform (Deans, 2007) to detect the vertical asymptotical lines, then adopted the image projection to read the parameters. If two vertical asymptotical lines are detected, they will be identified as ordinary and extraordinary traces; but if only one vertical asymptotical line is detected, the distance from this line to the extracted F layer ordinary trace will be calculated to determine whether it belongs to the ordinary trace or not.

The automatic scaling results of the F layer are shown in Fig. 8 and the scaled parameters are marked in blue horizontal and vertical lines.

6. Comparison with the manual method and discussion

To test the performance of the proposed method, we randomly selected a wide dataset of ionograms recorded by the digital ionosondes installed at three ionospheric stations (Xinxiang, Xi'an and Kunming) in different seasons and time listed below:

1. Subset A: 240 ionograms of Xinxiang station (35.267N, 113.934E) from 1st, 8th, 15th, 22nd, 30th April 2011 and 1st, 8th, 15th, 22nd, 31st October 2011.

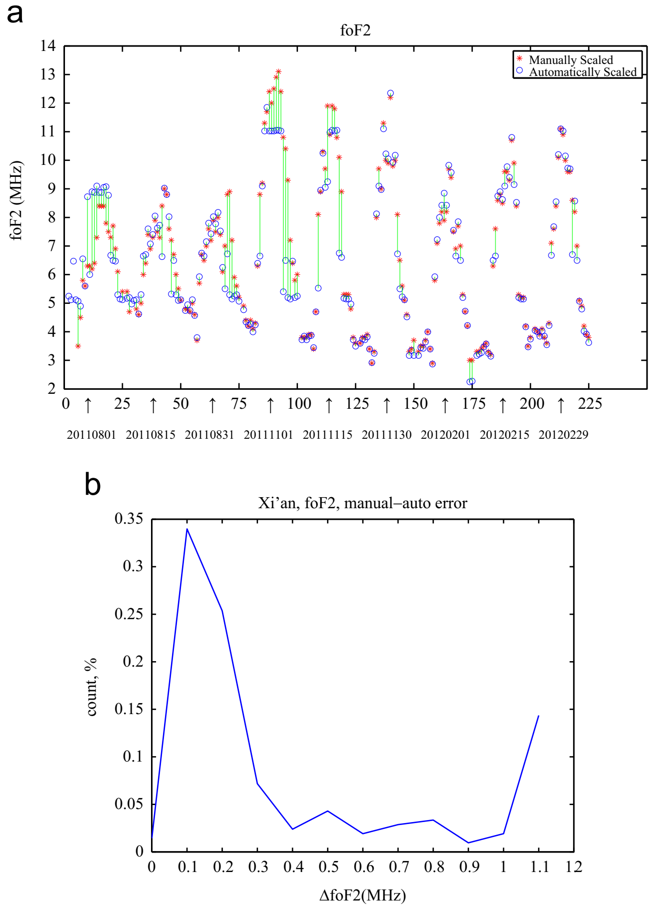

Fig. 9. foF2 comparison from Subset B. (a) The scaled results by our method (in blue circle) compared with that scaled by an experienced operator (in red asterisk), and the length of green vertical lines indicates the extent of the errors. (b) Errors Δ foF2. (For interpretation of the references to color in this figure caption, the reader is referred to the web version of this paper.)

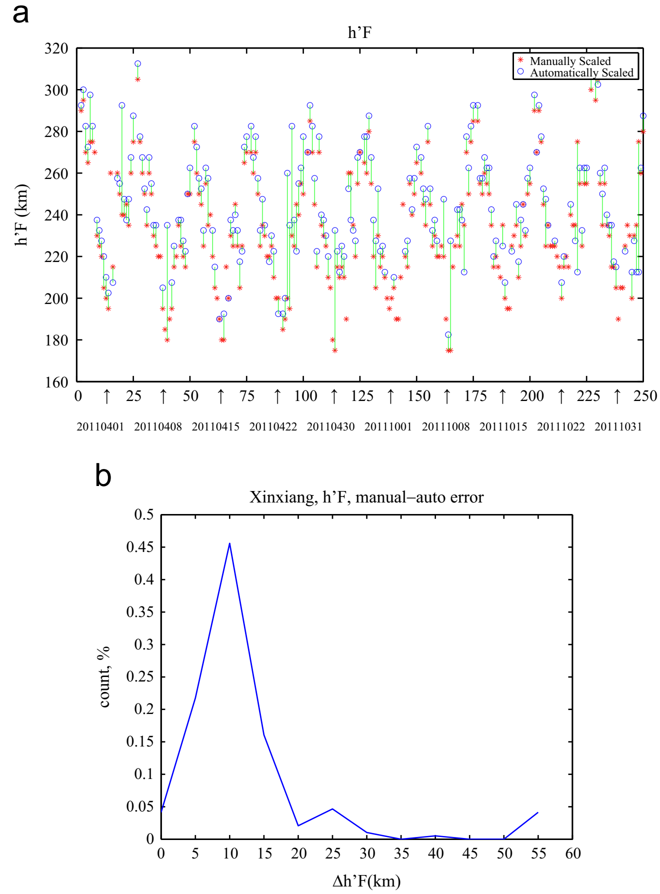

Fig. 10. h'F comparison from Subset A. (a) The scaled results by our method (in blue circle) compared with that scaled by an experienced operator (in red asterisk), and the length of green vertical lines indicates the extent of the errors. (b) Errors Δh'F. (For interpretation of the references to color in this figure caption, the reader is referred to the web version of this paper.)

2. Subset B: 216 ionograms of Xi'an station from (34.13N, 108.827E) 1st, 15th, 30th August 2011, 1st, 15th, 30th November 2011 and 1st, 15th, 29th February 2012.
3. Subset C: 240 ionograms of Kunming station (25.637N, 103.718E) from 1st, 8th, 15th, 22nd, 31st March 2011 and 1st, 8th, 15th, 22nd, 31st December 2011.

These random datasets, including the ionograms in different ionospheric conditions without any artificial selection or classification for different qualities, are automatically scaled by our method and manually scaled by an experienced operator. As the performance measures foF2 and h'F that appear in most day- and night-time ionograms are chosen to show the comparison as follows.

6.1. Comparison in errors

From Figs. 9b and 10b it can be shown that the number of foF2 errors above 0.1 MHz and h'F errors above 10 km are quickly reduced, which means that most of the errors are distributed in the nearby of 0.1 MHz for foF2 and 10 km for h'F.

From Fig. 9a, it can be seen that the errors of foF2 always appear temporally continuous, which may be caused by the ionosonde or other constant interference. As for the comparison of h'F from Fig. 10a, the lower part indicates the scaling errors of our method in the daytime resulting from the skeleton and fitting procedures as well as the discontinuity of the F layer trace. Besides, the big discontinuity of the F layer trace, the appearance of the Es blanketing as well as the Es layer multiple reflections can result in big errors of the F layer parameters such as the error over 1 MHz for foF2 in Fig. 9b and the error over 50 km for h'F in Fig. 10b.

Table 1
Correct rate of foF2 in different confidence levels ($\Delta = 0.1$ MHz).

Confidence level	Correct	Incorrect	Correct rate (%)
0Δ	22	820	2.6
1Δ	338	504	40.1
2Δ	524	318	62.2
3Δ	591	251	70.2
4Δ	633	209	75.2
5Δ	679	163	80.6
6Δ	704	138	83.6
7Δ	720	122	85.5
8Δ	732	110	86.9
9Δ	737	105	87.5
10Δ	746	96	88.6

6.2. Correct rates in different confidence levels

Different confidence levels ($0\Delta \sim \pm 10\Delta$, Δ is the reading accuracy, frequency is 0.1 MHz and height is 5 km) are used to

Table 2
Correct rate of h'F in different confidence levels ($\Delta = 5$ km).

Confidence level	Correct	Incorrect	Correct rate (%)
0Δ	24	704	3.3
1Δ	287	441	39.4
2Δ	534	194	73.4
3Δ	603	125	82.8
4Δ	627	101	86.1
5Δ	647	81	88.9
6Δ	659	69	90.5
7Δ	669	59	91.9
8Δ	676	52	92.9
9Δ	680	48	93.4
10Δ	687	41	94.4

evaluate the performance of our automatic scaling method in comparison with the manual scaling method. Because empty scaling results of parameters that the corresponding traces may not present in the ionograms were not considered in this experiment, the number of available ionograms (total 912) for foF2 and h'F are 842 and 728 respectively.

In this work an acceptable value is considered to lie within $\pm 5\Delta$ of the manual value. Such limits of acceptability were adopted in line with the URSI limits of $\pm 5\Delta$ (Pezzopane and Scotto, 2005). The results in Tables 1 and 2 show that the correct rate of foF2 and h'F within $\pm 5\Delta$ is all over 80%, which are valid and acceptable.

6.3. Discussion

The experimental results compared with the manual method show that the method we proposed in this paper is feasible to scale the F layer from ionograms automatically, but it needs further improvement to replace an experienced manual scaler. The accuracy of parameters (e.g. foF2) published from the other working automatic procedures such as ARTIST (Galkin and Reinisch, 2008) and Autoscala (Krasheninnikov et al., 2010) indicates a better scaling results. There are two factors that may affect the accuracy of automatic scaling: the datasets for test and the method. Although the empirical model can perform well, it is hard to be applied in a new ionospheric station directly as well as hard to “know” the specific situations that the model did not consider, which is a goal of this research work. Further efforts in this development might be directed toward the combination of image analysis and pattern recognition to “see” and “know” various ionospheric layer traces from ionograms.

There exist some problems that may impact the automatic scaling method presented in this paper: ionospheric disturbances causing multiples and magnetoionic components to differ; sporadic E multiples; spread-F; excessive interference and weak traces; poorly defined F1–F2 discontinuity due to ill-defined F1 cusp. For the multiples, the multiple relation of virtual heights and the similarity of the shape can be used to separate them; the density of the echo signals may be useful for identifying the spread F, then the edge detection technique can be adopted to scale the parameters; as for the excessive interference and weak or discontinuous traces, it may be useful to refer to the scaling results of the ionograms before and after, which is also adopted by the experienced manual scaler.

7. Conclusions

The long term goal of this work is a robust automated system for identification, extraction, and scaling of ionospheric layers on ionograms from different ionosondes at different longitudes and latitudes in different seasons and time. This paper is mainly concerned with the automatic scaling of the F layer from ionograms recorded by the digital ionosondes developed at China Research Institute of Radiowave Propagation. Special emphasis was placed on scaling the ionospheric F layer automatically without any empirical data or model and polarization information. Tests were performed comparing with the manual method and the obtained results were rather encouraging, which indicate that our method is feasible and will be used to develop a robust automated scaling system. Automatic scaling of the E layer from ionograms and applications to a wider range of ionograms containing specific disturbed ionospheric conditions will be our future work.

Acknowledgment

The authors wish to thank Hongguang Lu from China Research Institute of Radiowave Propagation for providing necessary assistance on the interpretation and reduction of ionograms. The authors also would like to thank the anonymous reviewers for their useful comments and language editing which have greatly improved the manuscript. This work was supported by “the Fundamental Research Funds for the Central Universities” (Grant no. 201313011, Ocean University of China).

References

Deans, S.R., 2007. The Radon Transform and Some of Its Applications. Dover Publications, Mineola, NY.

Ding, Z., Ning, B., Wan, W., 2007a. Real-time automatic scaling and analysis of ionospheric ionogram parameters. Chinese Journal of Geophysics 50, 969–978.

Ding, Z., Ning, B., Wan, W., Liu, L., 2007b. Automatic scaling of F2-layer parameters from ionograms based on the empirical orthogonal function (EOF) analysis of ionospheric electron density. Earth, Planets and Space 59, 51–58.

Fox, M.W., Blundell, C., 1989. Automatic scaling of digital ionograms. Radio Science 24, 747–761.

Galkin, I.A., Reinisch, B.W., 2008. The new ARTIST 5 for all digisondes. ⟨http://www.ips.gov.au/IPSHosted/INAG/web-69/2008/artist5-inag.pdf⟩.

Gonzalez, R.C., Woods, R.E., 2008. Digital Image Processing, 3rd ed. Prentice Hall, Upper Saddle River, NJ.

Igi, S., Nozaki, K., Nagayama, M., Ohtani, A., Kato, H., Igarashi, K., 1993. Automatic ionogram processing systems in Japan, in: Proceedings of Session G6 at the XXIVth General Assembly of the International Union of Radio Science.

Ji, G.R., Qiao, X.Y., Zheng, H.Y., Yuan, P., 2010. Feature extraction of Chaetoceros microscopic image based on skeleton. Periodical of Ocean University of China 40, 129–133.

Krasheninnikov, I., Pezzopane, M., Scotto, C., 2010. Application of Autoscala to ionograms recorded by the AIS-Parus ionosonde. Computers & Geosciences 36, 628–635.

Liu, W., Kong, Q., Chen, Y., Fan, J., 2009. Method on ionogram autoscaling based on IRI model. Chinese Journal of Radio Science 24, 218–223.

Otsu, N., 1979. A threshold selection method from gray-level histograms. IEEE Transactions on Systems, Man and Cybernetics 9, 62–66.

Pezzopane, M., Scotto, C., 2005. The INGV software for the automatic scaling of fof2 and MUF(3000)F2 from ionograms: a performance comparison with ARTIST 4.01 from Rome data. Journal of Atmospheric and Solar-Terrestrial Physics 67, 1063–1073.

Pezzopane, M., Scotto, C., 2008. A method for automatic scaling of F1 critical frequencies from ionograms. Radio Science 43, RS2S91.

Pezzopane, M., Scotto, C., 2010. Highlighting the F2 trace on an ionogram to improve Autoscala performance. Computers & Geosciences 36, 1168–1177.

Reinisch, B.W., Huang, X., 1983. Automatic calculation of electron density profiles from digital ionograms: 3. Processing of bottomside ionograms. Radio Science 18, 477–492.

Reinisch, B.W., Huang, X., Galkin, I.A., Paznukhov, V., Kozlov, A., 2005. Recent advances in real-time analysis of ionograms and ionospheric drift measurements with digisondes. Journal of Atmospheric and Solar-Terrestrial Physics 67, 1054–1062.

Samet, H., Tamminen, M., 1988. Efficient component labeling of images of arbitrary dimension represented by linear bintrees. IEEE Transactions on Pattern Analysis and Machine Intelligence 10, 579–586.

Scotto, C., 2001. A method for processing ionograms based on correlation technique. Physics and Chemistry of the Earth, Part C: Solar, Terrestrial & Planetary Science 26, 367–371.

Scotto, C., Pezzopane, M., 2002. A software for automatic scaling of foF2 and MUF (3000)F2 from ionograms, in: Proceedings of International Union of Radio Science XXVIIth General Assembly.

Scotto, C., Pezzopane, M., 2007. A method for automatic scaling of sporadic E layers from ionograms. Radio Science 42, RS2012.
Scotto, C., Pezzopane, M., 2008. Removing multiple reflections from the F2 layer to improve Autoscala performance. Journal of Atmospheric and Solar-Terrestrial Physics 70, 1929–1934.
Tsai, L.C., Berkey, F.T., 2000. Ionogram analysis using fuzzy segmentation and connectedness techniques. Radio Science 35, 1173–1186.
Zhang, T.Y., Suen, C.Y., 1984. A fast parallel algorithm for thinning digital patterns. Communications of the ACM 27, 236–239.